SUPPLEMENTARY MATERIAL

SUPPLEMENTARY METHODS

ANTIBODIES AND REAGENTS

The following antibodies and reagents were purchased: p16 (orb228122; Biorbyt, San Francisco, CA), phospho-ERK5 S496 (orb5183; Biorbyt, San Francisco, CA), NRF2 (GTX103322; Gentex, Irvine, CA), thioredoxin (TRX, 14999-1 AP20; Proteintech, Rosemont, IL), p90RSK (MAB 2056; R&D Systems, Minneapolis, MN), α-tubulin (T5168; Sigma-Aldrich, St. Louis, MO); phospho-ERK5 TEY (3371; Cell Signaling Technology, Beverly, MA), ERK5 (3372; Cell Signaling Technology, Beverly, MA), phospho-p90RSK (9341; Cell Signaling Technology, Beverly, MA), p21 (2947; Cell Signaling Technology, Beverly, MA), p53 (9282; Cell Signaling Technology, Beverly, MA), heme oxygenase 1 (HO-1, ab13248; Abcam, Cambridge, MA), DNMT3A (NB12013888; Novus Biologicals, Centennial, CO), TNFα (NBP1-9532; Novus Biologicals, Centennial, CO), 53BP1 (NB100-304; Novus Biologicals, Centennial, CO), KLF2 (NBP2-61812; Novus Biologicals, Centennial, CO), GAS6 (BS-7549R; Bioss, Woburn, MA), Ki67 (ab92742; Abcam, Cambridge, MA), CD36 (100011, Cayman chemicals, Ann Arbor, MI), AHR (MA1-514; Invitrogen, Carlsbad, CA), PCNA (13-3900; Invitrogen, Carlsbad, CA), SUMO2/3 (M114-3, MBL Life Sciences, Woburn, MA), and Lamin B (LS-C82208; LSBio, Seattle, WA). CD11b (553310; BD Biosciences), and F4/80 (565410; BD Biosciences).

Protease inhibitor cocktail (p8340; Tocris (Minneapolis, MN), PMSF (36978; Tocris (Minneapolis, MN); NEM (E3876; Tocris (Minneapolis, MN); AX15836 (5843; Tocris, Minneapolis, MN); XMD 8-92 (S7525; Selleck chemicals, Houston, Tx); Lipofectamine 2000 transfection reagent (11668027; ThermoFisher Scientific, Waltham, MA); Mitosox Red (M36008; ThermoFisher Scientific, Waltham, MA); MitoNeoD (563761; MedKoo Biosciences, Inc, Morrisville, NC).

The ATP assay kit (ab83355; Abcam, Cambridge, MA), GM-CSF (415-ML-050/CF; R&D Systems, Minneapolis, MN); Seahorse XF Cell Mito Stress Test Kit (103015-100; Agilent Technology, Santa Clara, CA); Seahorse XF Glycolysis Stress Test (103020-100; Agilent Technology, Santa Clara, CA); Seahorse XF Base Medium (103334-100; Agilent Technology, Santa Clara, CA); Seahorse XF24 FluxPak mini (100867-100; Agilent Technology, Santa Clara, CA); ARE reporter kit (60514; BPS Biosciences, San Diego, CA); Chemiluminescence detection reagent kit (NEL105001EA; PerkinElmer, Waltham, MA); ApopTag peroxidase in situ apoptosis detection kit (S7100; Millipore, Burlington, MA); Efferocytosis kit (4649; Essen Biosciences, Ann Arbor, MI); NAD/NADH-Glo kit (G9071; Promega™ Corporation, Madison, MI).

AHR siRNA (SR427538; Origene Technologies, Rockville, MD).

The antibodies used in imaging mass cytometry (IMC) were described in Supplementary Table 1.

RRID number for each antibody, cells, software tools, mice, and plasmids were described in Supplementary Table 4.

CONTACT FOR REAGENT AND RESOURCE SHARING

Further information and requests for resources and reagents should be directed to and will be fulfilled by the Lead Contacts, Jun-ichi Abe (jabe@mdanderson.org) or Sivareddy Kotla (skotla@mdanderson.org).

EXPERIMENTAL MODEL AND SUBJECT DETAILS

In this study, all animal procedures were performed in compliance with institutional guidelines and in accordance with research protocols approved by the Institutional Care and Use Committees of the Texas A&M Institute of Biosciences and Technology (2014-0231, 2017-0154) and The University of Texas MD Anderson Cancer Center (00001652, 00001109).

Generation of the ERK5 S496A KI mice:

Mice containing ERK5 S496A point mutation (C57BL/6 background) were generated using the CRISPR/Cas technique. A detailed description of the method can be found in our two recent papers[1, 2]. For confirmation of genotype, we performed PCR on genomic DNA from all pups, and the PCR products were sequenced to identify the correct point mutation and lack of any additional unwanted mutations surrounding the site of homology-directed mutagenesis. The primer pair used for PCR were 5'-TCTAGCAGGCTTCGGTCATTGTC-3' (forward) and 5'-TGCACCTGACACCGTTGATC-3' (reverse). For Sanger sequencing of the PCR product, the primer 5'-AGGGTGCCATCTCCGACAATAC-3' was used.

Housing and Husbandry:

Mice were housed in pathogen-free conditions at The University of Texas MD Anderson Cancer Center. The Program for Animal Resources is an AAALAC certified and defined pathogen-free facility for housing mice and rats[3]. A cage-level barrier system was used with an irradiated diet, ultra-filtered water, and heat-treated wood chip bedding. Enrichment material (nestlets) was provided. Cages and water were changed on a weekly basis. Animals were handled under a HEPA-filtered change station. Environmental parameters (ambient lighting, temperature, and humidity) were computer monitored as follows: 1) temperature: set point=22.2 °C (high limit=23.3 °C, low limit=21.1 °C), 2) humidity: set point=45% (high limit=55% and low limit=40%), 3) light-dark cycle: 12 hours of continuous light and 12 hours of continuous darkness, and 4) air exchanges 10-15 times per hour. The vivarium was staffed 7 days a week by animal caretakers, including weekends and holidays. Veterinary care and oversight were provided by a contract veterinarian who visited the facilities regularly and was available for consultation by phone or email.

Echocardiography:

Cardiac function was assessed in *ERK5* S496A KI and wild type (WT) C57BL/6 control mice on a high-fat diet (HFD) for 16 weeks after each received a single injection of adeno-associated-virus-8 overexpressing pro-protein convertase subtilisin/Kexin type 9 gain-of-function D377Y mutant (AAV8-PCSK9) at the age of 8-10 weeks as we previously described [4]. Echocardiograms of anesthetized mice were obtained using a Vevo2100 echocardiography machine equipped with an MS-550D 40-MHz frequency probe (VisualSonics). We performed anesthesia using 0.5-1 % isoflurane to maintain the heart rate at around 550 bpm for reducing suffering and distress. Left ventricular (LV) systolic and diastolic dimensions were measured in M-mode along the parasternal short axis of the LV. Fractional shortening was calculated using the following formula: %FS = 100% × (LV end-diastolic diameter − LV end-systolic diameter)/(LV end-diastolic diameter)[5].

Tissue Preparation, Histologic Evaluation, and Quantification of Lesion Size in Conventional Model of Atherosclerosis in Mice Induced by AAV8-PCSK9 Transduction:

In this model, we used only male mice for evaluating atherosclerotic lesions, because the size of atherosclerosis lesion was different between female and male. We randomly selected the mice from the pool of wild-type and ERK5 S496A KI male mice. We obtained rAAV plasmids encoding gain-of-function forms of murine *Pcsk9* (pAAV/D377Y-mPCSK9) from Addgene (plasmid #58376)[6]. PCSK9 expression was driven by an efficient liver-specific promoter, HCEApoE/hAAT. Viral vectors in serotype 8 capsids rAAV8-D377Y-mPCSK9 were produced by the University of North Carolina Vector Core (Chapel Hill, NC). Viral vectors (1×10^{11} titer/mouse) were delivered via a single tail vein injection into WT or ERK5 S496A mice at the age of 8-10 weeks; these animals had been fed an adjusted-calorie (high-fat) diet (HFD) consisting of 21% crude fat, 0.15% cholesterol, and 19.5% casein (TD.88137; Envigo, NJ)[7] for 16 weeks and then euthanized by CO_2 inhalation. In this AAV-PCSK9 injection model, according to the exclusion criteria established prior to the experiments, we excluded mice with LDL cholesterol level less than 300mg/dL after 16 weeks of HFD. The weight of each mouse was shown in Supplementary Fig. 1B.

Attrition: We excluded total 4 mice with LDL cholesterol level less than 300mg/dL after 16 weeks of HFD.

The arterial tree was perfused via the left ventricle with saline containing heparin (40 USPU/mL), followed by 10% neutral-buffered formalin in PBS for 10 minutes. The whole aortas and hearts of the mice were isolated. The full length of the aorta from the heart to the iliac bifurcation was dissected and opened along the ventral midline. *En face* preparations were washed in PBS, dipped in 60% isopropyl alcohol, and stained for 30 minutes with 0.3% Oil-Red-O that had been dissolved in 60% isopropyl alcohol. Stained images were captured with a digital camera mounted on a Nikon SMZ1000 stereomicroscope and analyzed using ImageJ software.

The aortic sinus area attached to the heart was dissected after fixation, and then embedded in paraffin. To examine the atherosclerotic lesions in the aortic valve area and necrotic core formation, serial sections (5 μm) were taken throughout the entire aortic valve area and stained with hematoxylin and eosin (H&E) to assess the quantification of atherosclerotic plaque as we described previously[7]. We traced the internal elastic lamina and luminal boundary of the lesion manually and the lesion sizes of the aortic root were quantified by ImageJ software. To quantify necrotic core formation, we made serial sections through the entire aortic valve area and stained them with hematoxylin and eosin; the necrotic core area was quantified by the percentage of the non-cellular area and total lesion area using ImageJ software (http://imagej.nih.gov/ij/). The necrotic core area can be determined by examination of the acellular regions of these stained sections as previously reported[8-10], and the necrotic core area was quantified as the percentage of the non-cellular area over the total lesion area. To prevent bias, the persons who evaluated the size of the plaque were blinded to the origin of the number of coded samples, not knowing the mouse genotypes and experimental conditions.

Hematoxylin and Eosin Staining:

We fixed the slides in 10% buffered formalin for 15 min and washed them in double-distilled water (ddH_2O). Next, we stained the slides with 0.1% hematoxylin for 3min followed by ddH_2O washes, 95% ethyl alcohol, and ddH_2O. Then we dipped the slides in 0.5% Eosin for 3 min, quickly rinsed with

ddH$_2$O, dipped in 95% and 100% ethanol, incubated in 50:50 Xylenes:100% ethanol, and lastly incubated in 100% Xylenes. We mounted the slides using Permount with coverslips.

Immunofluorescence staining:

The aortic valve area sections were incubated for 1 hour at 60 °C, deparaffinized in fresh xylene, and rehydrated through a graded alcohol series. After being washed with PBS, antigen retrieval was performed for 12 minutes at 95 °C in 10 mM sodium citrate buffer (pH 6.0) containing 0.05% Tween 20. Slides were washed with PBS and treated with Dako Protein Block Serum-free (#S3020, Dako) containing 10% normal goat serum for 1 hour at ambient temperature to block non-specific antibody binding. The slides were incubated overnight at 4 °C with anti-MAC3 antibody (#550292, BD Biosciences; San Jose, CA) and anti-p53 antibody (#ab131442, abcam) or anti-TRX antibody (#14999-1-AP, Proteintech) or anti-DNMT3a antibody (#NB120-13888, Novus). After being washed with PBS-T (PBS containing 0.2% Tween 20) and PBS, the slides were incubated with Alexa488 anti-Rabbit secondary antibody (1:2000, #A11055, Invitrogen) or Alexa488 anti-Mouse secondary antibody (1:2000, #A11029, Invitrogen), Alexa546 anti-Rat secondary antibody (1:2000, #A11081, Invitrogen), and DAPI (2.5 ug/mL, #D1306, Invitrogen) for 1 hour at ambient temperature. After being washed with PBS-T (PBS containing 0.2% Tween 20) and PBS, the cover slips were mounted. Immunofluorescence images of heart sections were captured by Olympus FX1200 MPE confocal laser scanning microscope.

Representative Image selection:

Representative images were selected based on the most accurate representation of similarity with the mean value of each experimental group from all experiments performed for each experiment and group, which were evaluated in a blinded manner.

Mouse Monocyte and Macrophage Culture:

Bone marrow cells were isolated by flushing the femurs and tibias of C57BL/6 WT mice (000664; Jackson Laboratory) or ERK5 S496A KI mice on the C57BL/6 background under a normal chow diet or after 4 months of an HFD and AAV-PCSK9 injection as described previously[2] and in each figure legend, and differentiated into macrophages by culturing at a density of $1x10^6$ cells/mL in Iscove's Modified Dulbecco's Medium (IMDM) (#13390, Sigma-Aldrich, St. Louis, MO) containing 10% fetal bovine serum (FBS), 10% (v/v) spent medium of L929 cell (NCTC clone 929 CCL-1™; ATCC, Manassas, VA) cultures as the source of macrophage colony-stimulating factor [11], 1% HEPES, and 1% penicillin-streptomycin for 5-8 days at 37 °C and 5% CO_2 in air.

Cell Line Authentication:

BMDMs were validated by flow cytometry and were typically >90% $CD11b^+$ and F4/80.

METHOD DETAILS

Transfection:

Cells were transfected with the appropriate plasmid DNAs using Lipofectamine 2000 transfection reagent according to the manufacturer's instructions. After transfection, cells were allowed to recover in the complete medium for 24 hours.

Western Blot Analysis:

Cells were washed twice with cold PBS, and whole-cell lysates were prepared in RIPA buffer (50 mM Tris-HCl [pH 7.4], 150 mM NaCl, 1 mM EDTA, 1% Nonidet P40, 0.1% SDS, 1 mM dithiothreitol, 1:200-diluted protease inhibitor cocktail [P8340, Sigma-Aldrich], and 1 mM PMSF), western blot analysis was performed as we described previously[2]. Tubulin was used as the loading control and was always probed together with the specific protein of interest. In most cases, tubulin immunoblots were not shown to save space. To obtain a fold-increase value, the intensity of each band was measured by Image J, and the mean intensity (integrated optical density) at the baseline (control) for each experiment was calculated from more than or equal to 5 replicates, then normalized to tubulin expression and designated as 1. We calculated a fold increase from this mean intensity at the control with every band's intensity performed in each experiment.

Immunoprecipitation (SUMO assay):

Cells were collected in PBS containing 10 mM N-ethylmaleimide (NEM), and cell extracts were prepared in SUMOylation buffer (50mM Tris-HCl, pH 7.4; 150 mM NaCl; 1 mM EDTA; 1 mM EGTA; 1% Nonidet P-40; 0.1% sodium dodecyl sulfate (SDS); 0.25% Sodium Deoxycholate; 1 mM Na_3VO_4; 1:200-diluted protease inhibitor cocktail (Sigma, St.Louis, MO); 1 mM PMSF; and 10 mM NEM). SUMOylation was detected by immunoprecipitation analysis as previously described[12]. Briefly, Cell lysates were centrifuged at 12,000 g for 30 min at 4 °C. Protein concentrations were determined by a BCA protein quantification assay kit (Pierce). 0.5 mg lysates were immunoprecipitated with a polyclonal rabbit anti-NRF2 (GTX103322; Gentex, Irvine, CA) or anti-rabbit IgG (ab37415; abcam) and incubated overnight at 4 °C. After that, 40 ul of the Protein A/G Dyna beads were added to the antibody-protein mixture and incubated for 4 hrs at 4^0C. Immunocomplexes were separated by a magnet stand followed by five washes with SUMOylation lysis buffer and subjected to Western blotting with mouse anti-SUMO2/3.

Real-time PCR (qRT-PCR):

At the end of experiments, cells were washed 3 times with PBS and total RNA was isolated with TRIzol reagent (Invitrogen, #15596026). qTR-PCR was performed as we previously described[2]. Each reaction mixture (10μl) contained cDNA synthesized from 20 ng of total RNA, 5 μl of iQ SYBR Green Supermix (1708882; Bio-Rad, Hercules, CA 94547), and 0.5 μmol/l each of forward and reverse primer (IDT) with qSTAR quantitative PCR primers shown in Supplemental Table. Reactions were performed in triplicate. qRT-PCR data acquisition was carried out using the CFX96 TouchTm Real Time detection System (Bio-Rad) and SYBR Green (Bio-Rad) at thermal activation for 10 minutes at 95°C and 40 cycles of PCR (melting for 15 seconds at 95°C, followed by annealing/extension for 1 minute at 60°C). The comparative C_t ($^{2-\Delta\Delta Ct}$) method was used to relatively quantified changes in mRNA expression of samples, in which cycle threshold (Ct) values of target genes were normalized to that of the reference genes[13]. All qRT-PCR primers were obtained from Sigma-Aldrich. The sequences of qRT-PCR primers were listed in the Supplementary Table 1.

Efferocytosis Assay:

BMDMs were cultured in IMDM containing 10% (v/v) FBS (Hyclone), 1% HEPES, and 1% penicillin-streptomycin, efferocytosis assay was performed as we described previously. [2] We measured efferocytotic activity using IncuCyte ZOOM live cell imaging (ESSEN Bioscience, Ann Arbor, MI). Engulfment of pHrodo-labeled cells induces pHrodo fluorescence by the phagosome's acidic environment, and the fluorescence intensity of the image was determined using IncuCyte ZOOM, as we previously reported[14].

ATP Assay:
Intracellular ATP concentrations were measured using the ATP Assay Kit Colorimetric/Fluorometric (Abcam ab83355) per the manufacturer's protocol.

Metabolic Extracellular Flux Analysis (Seahorse):
25,000 BMDMs/well were seeded into Seahorse XF24 cell culture microplates 16 hours before the assay and cultured with XF medium. Then, cells were cultured in Seahorse XF Base Medium supplemented with 1 mM pyruvate, 2 mM glutamine, and 10 mM D-glucose for the Seahorse XF cell mito stress test and with 1 mM glutamine for the Seahorse XF glycolysis stress test. The cell culture microplate was placed in a 37 °C non-CO_2 incubator for 1 hour and then loaded onto Seahorse XF24 to measure OCR and ECAR using a Seahorse XF24 Extracellular Flux Analyzer (Agilent, Santa Clara, CA) as we described previously[2].

ERK5 Transcriptional Activity:
We detected ERK5 transcriptional activity as we described previously[2, 14].

NRF2-ARE Transcriptional Activity:
We detected NRF2-ARE transcriptional activity as we described previously[14]. Transfections were performed in triplicate, and each experiment was repeated at least 5 times.

NF-κB Activity:
NF-kB activity was measured as we previously described[2]. BMDMs were transfected with a mixture of the NF-κB-Luc and pRL-TK vectors (encoding Renilla luciferase) using Lipofectamine 2000 in Opti-MEM according to the manufacturer's instructions. The cells were harvested and assayed for firefly and Renilla luciferase activity using the Promega Dual-Luciferase Reporter Assay System.

Mitochondria-Specific ROS Measurements (MitoNeoD and MitoSOX Red):
We measured mitochondria-specific ROS as we described previously[2, 14]. In brief, cells were incubated with MitoSOX Red (5 μM) (#M36008, Invitrogen, Eugene, OR), and fluorescence intensity was measured with excitation at 510 nm and emission at 580 nm using a plate reader (FLUOstar Omega, BMG LABTECH,Cary, NC). We set the mean level at control = 1, and calculate the "fold increase" for each measurement.

Since the non-specific detection of MitoSOX Red has been suggested, we also performed MitoNeoD methods to detect mitochondrial ROS[15]. MitoNeoD contains an $O_2^{\bullet-}$-sensitive reduced phenanthridinium moiety modified to prevent DNA intercalation. A carbon-deuterium bond enhances MitoNeoD's selectivity for $O_2^{\bullet-}$ over non-specific oxidation. Lastly, a triphenylphosphonium lipophilic cation moiety of MitoNeoD induces rapid accumulation within mitochondria. Cells were seeded into 96 -well black, clear-bottom tissue culture plates at 10,000 cells per well and were treated as indicated in each figure. After indicated time points, cells were washed with HBSS buffer, and incubated with 5μM MitoNeoD for 20 min at 37ºC. After washing three times with HBSS buffer, fluorescence intensities were measured using a plate reader (FLUOstar Omega-BMG LABTECH) with excitation, and emission wavelengths were 544 and 605 nm, respectively (MitoNeoD). The fluorescence intensity values of each unstained sample were subtracted from the fluorescence intensity values of the stained sample (either treated with

oxLDL or vehicle) to remove the background fluorescence and to obtain the net fluorescence intensity values. We set the stained sample's mean fluorescence intensity at control = 1, and calculate the "fold increase" for each measurement.

Migration assay in Boyden chambers:

Transwell assay was performed via Boyden chamber with 8.0μm pore size (Corning, CLS3422) as described previously[16]. The bottom chamber surface of the membrane was coated with 0.1% martigel (356234; BD Biosciences) for 30 min. BMDMs were incubated in serum-free IMDM medium at 37°C and 5% CO2 for 2 hours before the assay. Added 500 ul serum-free IMDM medium with oxLDL (10 μg/ml) or vehicle control to the lower chamber. BMDM (1.5×10^5 cells/mL) was added to the upper chamber and incubated at 37°C and 5% CO2 incubator for 20 h. After incubating at 37°C in 5% CO_2 for 20 hours, non-migrated cells were scraped from the upper surface of the filter. BMDMs on the lower surface were fixed with 4% paraformaldehyde for 20 minutes at room temperature, washed three times with PBS, and stained with crystal violet (0.1%; Sigma (Cat# V5265) for 20 min at room temperature. We determined the number of BMDMs on the lower surface of the filter by counting five random high-power (200×) fields of constant area per well by inverted microscope (BZ-X810; Keyence). Experiments were performed in triplicates, from five independent experiments.

In Situ TUNEL Assay:

TUNEL staining was performed using the ApoTag peroxidase *in situ* apoptosis detection kit (#S7100, Millipore) as we described previously[17].

Annexin V Apoptosis Assay:

Annexin V apoptosis assay was performed using annexin V-fluorescein isothiocyanate (annexin V-FITC apoptosis detection kit (ab14085, Abcam, Cambridge, MA) as we described previously[14].

Serum Lipid Profile Analysis:

The levels of cholesterol (HDL, LDL) were determined using a cholesterol assay kit for mice (EHDL-100, Bioassay System, Hayward, CA) as we described previously[14].

RNA-seq data analysis:

We used Top Hat program (v2.0.12) with default parameters to map all paired-end RNA-seq reads to the mouse genome (Mus musculus GRCm38). Gene expression and significance of DEGs were calculated by Cuffdiff (v2.0.12). DEGs were defined by Cuffdiff according to *Q* value ≤0.05 as a threshold. We calculated *p* value for each GO term with a modified Fisher's exact test on DAVID website (https://david-d.ncifcrf.gov). Hallmark analysis was performed by Gene Set Enrichment Analysis (GSEA v4.2.1). We used the R package "GOplot" to perform GO bubble plot, GO circle plot, and GO chord plot.

NAD^+ Measurement levels:

Total intracellular NAD+ was measured using the NAD/NADH-Glo Bioluminescent Assay Kit (G9072; Promega Corporation, United States), according to the manufacturer's instructions. BMDMs were lysed with dodecyl trimethyl ammonium bromide and treated to neutralize their counterparts. To measure NAD^+, the extract was treated with 25 μL of 0.4 N HCl and heated at 60°C for 15 min, incubated at RT for 10 min, following the addition of 25 μL Trizma base. Next, the equal volume of NAD/NADH-Glo TM detection reagent was added to each well and incubated for 30 minutes at room

temperature. The intensity of light (proportional to the amount of NAD^+) was detected by a luminometer (BGS Microplate Reader; BGS).

Cytokine Profile in Mouse serum:

Mouse Inflammatory Array (AAM-INF-1-4, Ray Biotech, Inc) were used according to the manufacturer's instructions. Cytokine array membranes were incubated in equal quantities of serum either from WT-HFD or ERK5S496A-HFD at 4^0C for overnight. After washing with wash buffer, membranes were incubated in biotin-labeled primary antibodies, followed by 1,000-fold diluted HRP-conjugated streptavidin added and developed. After development, films were scanned, and the images were processed and quantified using ImageJ software (National Institutes of Health). The relative intensity was quantified using densitometry with ImageJ software with reference to the positive controls on the membrane.

Senescence associated (SA) β-Galactosidase Activity in cell cultures:

β-galactosidase activity was detected in cells using by GlycoYELLOW™ - βGal Kit (SCTO24) from Millipore Sigma. β-galactosidase detection was carried out according to the manufacturer's instructions. The images were taken using Incucyte. SA-β-gal staining positive cells were quantified based on three independent images from different regions of the staining.

Flowcytometry of senescence associated cell stemness analysis:

BMDMs were treated with Bafilomycin A1, followed by incubation with C12FDG (Molecular Probes/ Life technologies), which is a fluorogenic substrate for β-gal activity, for 2 h at 37ºC with 5% CO_2 as described previously[18]. After that, cells were washed with PBS, harvested by scraping, centrifuged, and fixed with fixation buffer for 30 min at 4ºC. Cells were washed once with FACS staining buffer, centrifuged, and after discarding the supernatant, the pellet was suspended in permeabilization buffer and incubated for 5 min at 4ºC. After centrifugation, the pellet was resuspended in FACS staining buffer and incubated with anti-Ki67 primary antibody at 4^0C for 1 hr. Cells were washed three times and then incubated with a secondary antibody for 1 hr at room temperature, followed by three times washing and analyzed by flow cytometry. Data were analyzed using Flowjo software. Live cells were selected based on the side and forward scattered. Fluorescence-stained gates were set up based on the unstained samples, and compensation was set up based on single-stained controls. We also performed the p53BP1and Ki67 double staining for detecting double positive cells with anti-p53BP1 (NB100-304; Novus Biologicals, Centennial, CO) as described above.

Imaging Mass Cytometry (IMC)

The antibodies are conjugated with rare-earth-metal isotopes of defined atomic masses, which allows the antibody bound proteins to be separated by a mass cytometer. The tissue was laser-ablated spot by spot and line by line, and the ablated materials were transported to the CyTOF mass cytometer by a mixed argon and helium stream. The 23 transient and single isotope signals were plotted using the coordinates of each single laser shot; by overlaying all analyzed measurement channels as described previously[19]. The Fluidigm Hyperion Imaging system allows the simultaneous detection of >20 parameters in a single tissue sample while eliminating the common challenges of conventional immune-histochemical analysis, such as signal fading, auto-fluorescence, signal linearity, and spectral overlap.

Antibody panel for IMC and antibody conjugation

We used 26 antibodies and Ir DNA-Intercalator (Cell-ID Intercalator-Ir; Fluidigm #201192A) for IMC, as listed in Supplemental Table 1. The markers (Na/K ATPase, alpha smooth muscle actin and TCRβ, which are not included in Supplemental Table 1) showed no signal or non-specific staining and served as negative controls. The antibodies listed in Supplemental Table 1, except for the metal-conjugated antibodies that were purchased from Fluidigm, were conjugated to metals using the Maxpar X8 Multimetal Labeling Kit (Fluidigm) according to the manufacturer's protocol. To determine optimal antibody concentrations, 3 different concentrations of each metal-labeled antibody were tested by IMC prior to being used in antigen expression analyses (see below).

Tissue staining with metal-conjugated antibodies for IMC

Hearts were harvested and fixed for 24 hours in 10% formalin and embedded in paraffin after the dehydration procedure by an automated tissue processor (LEICA, TP1020). A paraffin tissue section microarray (TMA) was built using 7 independent WT samples and 6 independent ERK5 S496A KI samples from 3-mm 13 tissue block cores. The cores were embedded in a large paraffin block, which was then sectioned and mounted onto a TMA slide. The TMA slides consisted of tissues containing the aortic valve area, and the section thickness was 5 μm. H&E staining was performed to confirm that all cores have atherosclerotic plaques in the aortic valve area and to determine the position and size of atherosclerotic plaques.

TMA slides were incubated for 16 hours at 60 °C, deparaffinized in fresh xylene, and rehydrated through a graded alcohol series. After the slides were washed with TBS-T (TBS containing 0.1% Tween 20, pH 7.6) and TBS, antigen retrieval was performed for 15 minutes at 95 °C in 10 mM sodium citrate buffer (pH 6.0) containing 0.05% Tween 20. Slides were washed with TBS-T and TBS and treated with TBS containing 1% normal donkey serum and 3% BSA for 2 hours at ambient temperature to block non-specific antibody binding. The slides were incubated overnight at 4 °C with 26 metal-conjugated antibodies, as described in Supplemental Table 1. After being washed with TBS-T and TBS, the slides were incubated with 5 nM Ir DNA-Intercalator (Fluidigm) that had been diluted in TBS for 5 minutes at ambient temperature. After being washed with TBS and doubly distilled H_2O, the slides were immediately dried with pressurized air. After 1 or 2 days, the slides were scanned by the Hyperion Imaging System (Fluidigm), as described below.

IMC image acquisition

Regions of interest (ROIs) were chosen manually based on the plaque position and shape, which was identified by earlier H&E staining. Of note, between the WT cores and the ERK5 S496A KI cores, we intentionally selected similar plaque sizes for ROI because we intended to characterize the plaque composition of a similar plaque developmental stage.

Data acquisition was performed on a Helios time-of-flight mass cytometer coupled to a Hyperion Imaging System (Fluidigm). Prior to laser ablation, optical images of slides were acquired using Hyperion software, and the ROI to ablate was selected as described above. Laser ablation was performed at a resolution of approximately 1 μm and a frequency of 200 Hz. In total, 18 image stacks from 7 WT samples and 18 image stacks from 6 ERK5 S496A KI samples were acquired.

IMC data analysis

MCD format (.mcd) files that were generated after data acquisition were converted to multi-TIFF images using the MCD viewer (Fluidigm). The TIFF images were loaded using VIS software (Visiopharm; Hoersholm, Denmark) to generate the database. First, we created an analysis protocol package for cell segmentation, trained by the nuclear staining by Ir DNA-Intercalator, to define cell borders in the VIS software. After cell segmentation, we defined another analysis protocol package for phenotyping that was trained by the expression level information of functional markers and cell-type markers across all images. For some markers in the analysis protocol package, the threshold was applied to separate EC-like clusters and MC-like clusters. We analyzed 19,476 cells in WT ROIs and 14,680 cells in ERK5 S496A KI ROIs; 9 phenotypic clusters were identified in both WT and ERK5 S496A KI ROIs. To measure the expression level of each marker per cell and the distance among cells, we added the calculation of mean intensity of each marker in each cluster per cell and the calculation of object distance between 2 different clusters per cell into the output variable part of the analysis protocol package. After running the batch process containing all analysis protocol packages, we obtained the phenotype matrixes, the t-SNE plots, the intensity of each marker per cell, and the cell-cell distance information. We used GraphPad Prism 8 (GraphPad; San Diego, CA, USA) to create graphs and violin plots.

The intensity was determined using mass cytometer counts, which were scaled to 16-bit pixel values when the images were exported. These exports created the base intensity measurements for each pixel; the mean intensity in the cellular segmentation was calculated by accumulating pixels. We selected the molecules, which showed a median expression level >0.25 (intensity) in MCs and 0.19 (intensity) in ECs; the up-regulation and down-regulation of intensity between WT and ERK5 S496A KI mice were consistent among all the MC-like clusters. On the basis of the large IMC data set (n>500), the value that met both unpaired t test with Welch's correction $P<0.01$ and Mann Whitney test $P<0.01$ was considered statistically significant based on the previous recommendations[20, 21].

We analyzed key molecules that differentiate between the phenotype and functional status of endothelial cells and macrophages in relation to the atherosclerotic plaque. To determine the role of ERK5 S496 phosphorylation in regulating SASP and DDR events, we selected antibodies against the molecules associated with 1) senescence, 2) inflammation, 3) efferocytosis, 4) antioxidant, and 5) DDR that had demonstrated the normal distribution of their expression signals. The 26 transient and single isotope signals were plotted using the coordinates of each laser shot; by overlaying all analyzed measurement channels, we generated a high-dimensional image of the atherosclerotic plaques obtained from WT and ERK5 S496A KI mice. Using the VISIOPHARM program (Hoersholm, Denmark), we found that single-cell features were computationally segmented with a watershed algorithm (Fig. 2B).

Single cell marker or molecule expression data were extracted. These single-cell data were analyzed using the Phenomap module, which adds functionality for automatically clustering high-parameter datasets, generating t-SNE plots (Fig. 2D) and the phenotype or cluster matrix (Fig. 2E) using a clustering algorithm (each cluster's elements are shown in Figure 2E). Using the trained analysis protocol package, the unsupervised clustering algorithm across all images was used to divide identified cells into the identified clusters and further visualize them on a phenotypic matrix and tSNE plots. Of note, since we characterized cell composition and molecule expression in each plaque, we intentionally selected similar sized plaques from ERK5 S496A KI and WT mice for IMC analysis.

Power calculation:

Our preliminary studies showed the coefficient of covariation was about 30%. A sample size of 15 mice in each group was expected to have 90% power to detect an effect size of 1.226-SD at a two-sided significance level of 0.05 using two-sample t-test. The effect size of 1.226 corresponds to about 36% mean change between the two groups, for example, atherosclerosis lesion size between wild-type and ERK5 S496A KI groups.

Statistical Analysis:

Statistical analysis was performed using GraphPad Prism software ver. 9.0.0 (San Diego, CA, USA). First, we performed the Shapiro-Wilk test to check the normality of each group. Since the number was too large, we performed D'Agostino & Pearson test to check the normality of each group described in Fig. S2G. Comparisons among more than two groups were performed using ordinary one-way or two-way analysis of variance (ANOVA) followed by Tukey post hoc multiple comparisons test after the data passed the Shapiro-Wilk normality test. An unpaired Student's t-test (two-tailed) was applied for comparing the two groups also after the data passed the Shapiro-Wilk normality test. Data that failed the normality test, the Mann-Whitney U test was used to analyze two-group comparisons, and Kruskal-Wallis followed by Dunn post hoc multiple comparisons test for multi-group comparisons. *P* values <0.05 were considered statistically significant, except IMC data analysis, and are indicated by 1 asterisk in the figures. *P* values <0.01 are indicated by 2 asterisks. We performed all experiments independently unless specifically stated.

For analyzing Western blot analysis, we used ECL detected by CCD imager, and quantified Western blot based on the guideline described by Degasperi et al. [22] We divided all data points from a replicate by a normalization point in that replicate. The normalization point, which was the most reproducible condition, was selected. We selected medium-intensity points to avoid the lowest and highest-intensity data points based on the guideline described in Degasperi et al.[22] The normality assumption cannot be verified based on the data acquired in the study. However, we followed the guideline described by Degasperi et al.,[22] who reported that by following their guideline, we could obtain the data within a linear dynamic range, minimize the coefficient of variation of the normalized data, and assume the normality. We also published multiple papers and detected the expression of the same molecules in the same cells (bone marrow-derived macrophage) derived from ERK5 S496A KI and wild-type cells using the same Western blotting techniques and antibodies.[2, 14] Combining these data from our lab also supports the normality assumption of our Western blot data. Moreover, for Western blot experiments, since we obtained each experimental data set as an average of a large number of cultured cells, we assumed the data was normally distributed based on the central limit theorem.

For analyzing IMC data with the SAS group (Fig.3A-E), first, to exclude the non-senescent and proliferative cells (low p53 and low Ki67 MCs), we calculated the two-dimensional density of expression of Ki67 and p53 by "kde2d" function of R and selected cells to involve in the further analysis according to density<0.1 by using spatialEco R package[23] as shown in Fig.3A. In Figure 3A, 585 cells were grouped using the threshold of 0.1. To have a fair comparison, we set the number of cells to be grouped to 585 in Fig. S2H, I, and J, which has the same grouped cells number (585 cells) as shown in Fig. 3A. We ranked the density of each cell, and then obtained cells with the lowest 585 densities to be grouped. Next, to determine the different distribution pattern groups of the cells, we calculated log scaled ratio of Ki67 and p53 of selected cells by $\log_{10}$(expression of Ki67/ expression of

p53), and we further calculated the one-dimensional density of this log-transformed ratio. Because the one-dimensional density distribution of this parameter was trimodal, MCs can be divided into three groups based on different patterns of p53:Ki67 expression (Fig. 3A) and two groups (Fig.S2H and S2J) with the cutoff values -1.01 and -0.024 (Fig. 3B), -0.072 (Fig.S2H), and -0.633 (Fig.S2I), respectively. To calculate the significance of the proportion between WT and ERK5S496A in each group, we used the boosting algorithm. We sampled 500 cells from all cells to calculate the proportion of group 1, 2, and 3 by using base R package with the sample function. We repeated the sampling 1,000 times. Wilcoxon test was performed to estimate *p* values between wild type and knocked-in cells in three groups (Fig.3C-E).

Random effects modeling can be useful in the presence of hierarchical observations. As noted by Krzywinski, Altman, and Blainey[24], this modeling approach is useful for understanding sources of variability in the hierarchy of the subsamples and can reduce the cost of the experiment. Reductions in cost may occur if intra-class correlations are large. While partitioning sources of variability may be interesting when one cares about inferences at multiple levels of the hierarchy, choosing fixed effects ANOVA in our setting as an alternative should not be considered an invalid approach to analysis. Our inference is focused on the mean-shifts in distribution. As Krzywinski et al. noted[24], the random effects approach may provide more power (less false negatives for the same false positive rate). While we have conducted statistical analysis without partitioning the variance into hierarchical components (which is less powerful), we have numerous significant statistical findings, despite the reduction in power.

Please check the IMC method section for the statistical analysis with the IMC data set.

Statistical information, including the *n* of each group, the normality test results, the applied statistical methods, and *P* values for each figure, are summarized in Table S3.

Controls for each relative value:

Controls for each relative value were described in Supplementary Figure 4.

Data availability:

The RNA-seq data was deposited in the NCBI's Gene Expression Omnibus database (accession GSE210949). All other data supporting the findings of this study are available within the article or its supplemental materials.

Please see the Major Resources Table in the Supplemental Materials.

SUPPLEMENTARY DISCUSSION

One of the defining characteristics of senescent cells is their cell cycle arrest[25, 26]. The activation of two pathways of (p53/p21 and p16/Rb) plays a crucial role to control senescence-induced cell cycle arrest[25]. When we co-plotted p53 and Ki67, which is used as a proliferation marker in the atherosclerosis lesions [27], we found a clear relationship between p53 and Ki67 showing that p53 played a role in inducing cell cycle arrest in Groups 1 and 3 in myeloid cells (Fig. 3A), and also in vascular smooth muscle cells (VSMCs) (Fig. S2J). Milanovic et al. have defined SAS as "an unexpected, cell-autonomous feature that exerts its detrimental, highly aggressive growth potential upon escape from the cell-cycle blockade"[28]. Since p53 is a major cell-cycle blockade mechanism in macrophages during atherosclerosis formation[29], we investigated the relationship between p53 and Ki67 in the plaque. We found that some of the myeloid cells escape from the p53-mediated cell-cycle blockade, which was defined as Group 2 in Fig. 3A. One of the important characteristics of SAS is "escaping from cell-cycle arrest", and we found that in Group 2 MCs, p53 and Ki67 were linearly co-expressed ($y = 0.92x + 0.81;$ F test $p-$ value < 0.001). If p53 maintains its function as a cell-cycle blocker, the expression of p53 and Ki67 should not be linear as shown in Group 1 and 3 in both MCs and VSMCs. Group 1 had a high p53 expression-mediated anti-proliferation (low Ki67 level) whereas Group 3 had a low p53 expression-mediated high proliferative capacity (high Ki67 level) (Fig.3A). Of note, we did not observe the features of Group 2 in ECs (Fig. S2I) and VSMCs (Fig.S2J), indicating that SAS uniquely occurred in MCs.

In order to evaluate the induction of senescence in the plaque, we initially proposed to compare the vessels from the atherosclerotic and non-atherosclerotic mice. However, we realized that this is difficult because the cell composition differs between plaque and non-plaque intima. For instance, there are very few myeloid cells in the non-plaque intima[30, 31], and it is not practical to compare the MCs in the condition with such differences in cell numbers. It has been reported that circulating monocytes derived from bone marrow accumulate continuously during atherosclerosis formation, which strongly links to lesion size and hypercholesterolemia (HC)[30, 32]. Therefore, we compared the phenotypes of BMDMs from HC and non-HC mice, which reflects the phenotypes of the myeloid cells accumulated in the plaque. We found evidence for SASP induction in BMDMs isolated from HC mice. By using these BMDMs, we also evaluated two senescence markers (p53-binding protein 1 (53BP1) and LAMIN B1) and a cell growth marker (proliferating cell nuclear antigen (PCNA)) as evidence for SAS in HC-mediated reprogrammed BMDMs. We observed an increase of 53BP1 and PCNA, and a decrease of LAMIN B1 expression in HC WT-HFD mice (HFD BMDMs) compared to NC WT-NCD mice (NCD BMDMs) (Fig. 3F and Fig. S3). Furthermore, we also found double SAβ-gal and Ki67 positive (SA β-gal$^+$Ki67$^+$) (Fig. 3L, M), and double 53BP1 and Ki67 positive (53BP1$^+$Ki67$^+$) macrophages (Fig. 3N, O) from the HC WT-HFD mice (Fig. 3L-O). All these findings are suggestive of an induction of SAS by HC in myeloid cells.

Therefore, we have three lines of evidence supporting our hypothesis of induction of SAS by HC in myeloid cells: (1) the escape from the cell-cycle arrest as shown by linear co-expression of p53 and Ki67 in the plaque; (2) the induction of both SASP and proliferation markers in BMDMs from HFD BMDMs compared to those from NCD BMDMs; and (3) the existence of double positive macrophages of SA β-gal$^+$Ki67$^+$ 53BP1$^+$Ki67$^+$ from HFD BMDMs. We also plotted p16 and Ki67 in MCs *in vivo*. Although we did see some tendency for the existence of Groups 2 and 3, there was no evidence for a

Group 1. (Fig.S2H). Cudejko et al. have reported that p16 deficiency does not module macrophage cell-cycle progression[33]. Therefore, p16 is unlikely to play a key role in the regulation of macrophage proliferation. Also, p16 expression intensity was relatively lower than p53 expression (Fig.S2G), blurring the picture for Group 1.

We found the upregulation of p16 (#7 and #9) and p-PKCζ (#1, #7, and #9) expression in the ERK5 S496A KI group compared to those in the WT group. To determine the phenotypes of cells in the plaques of these two groups of mice, we intentionally selected a similar size of plaques for our IMC analysis, as we described in the methods, assuming that this would make a fairer comparison of the plaque cell phenotype in the two groups of mice. By doing so, however, it is possible that we have selected plaques in which the inflammatory response was augmented, probably by p16[34], PKCζ[35], and IL-6 induction, in the ERK5 S496A KI mice. Nevertheless, both KI and WT mice exhibited similar levels of regulation of p53, efferocytosis, antioxidants, and DNA damage response molecules' expression mediated by ERK5 S496 phosphorylation both *in vivo* (IMC data) and *in vitro* (cultured myeloid cells). These results suggest that neighboring cells' inflammatory conditions may play a critical role in p16 and other inflammatory molecules' expression in plaque macrophages as described previously[36]. Therefore, to detect phenotypic changes of macrophages in the plaque, it may be important to perform both *in vitro* and *in vivo* studies to exclude the temporal vessel environmental effects. Further investigation will be necessary to clarify these issues.

SUPPLEMENTARY FIGURE LEGENDS

Supplementary Figure 1. Body weights and serum cholesterol levels in ERK5 S496A KI mice after AAV-PCSK9 injection and fed a HFD *in vivo,* and mtROS detection by MitoSOX Red assay.

(A) WT BMDMs and ERK5 S496A KI BMDMs were treated with oxLDL (10 μg/ml) for 0-30 minutes, and a immunoblotting analysis was performed using antibodies against the indicated proteins *in vitro* (left). The right graph represents densitometry data from 3 independent gels, one of which is shown in the left panel. n=3 (time course). Body weight **(B)** and HDL and LDL levels **(C)** in ERK5 S496A KI and WT mice after AAV/D377Y-mPCSK9 injection and fed a HFD. Echocardiographic parameters in ERK5 S496A KI and WT mice after AAV/D377Y-mPCSK9 injection and fed an HFD, LV FS **(D)**: Left ventricular (LV) fractional shortening, LVPW;d **(E)**: LV end-diastolic posterior wall thickness. **(F, G)** WT BMDMs and ERK5 S496A KI BMDMs were incubated with oxLDL as indicated. mtROS levels were detected by MitoSOX Red as described in the methods section *in vitro*. Cells treated with oxLDL or MitoTEMPOL (10 μM) and vehicle control **(G)** were assayed 24 hours later. **(H)** BMDMs isolated from WT and ERK5 S496A KI mice fed a NCD or HFD for 4 months were cultured with the same medium *ex vivo,* and mtROS levels were detected by MitoSOX as described in Methods. **(I)** BMDMs were treated with indicated mutants and inhibitors as described in Fig.5, and mtROS production was detected by MitoSOX as described in the Methods. The applied statistical tests, sample number, and results in all figures are summarized in Table S3. All data are expressed as mean±SD.

Supplementary Figure 2. ERK5 S496A mutation and SASP components and DNMT3a in MCs ECs, and VSMCs *in vivo*.

(A-C) Traditional immunofluorescence staining strengthens the results obtained from IMC. To determine the p53, TRX, and DNMT3a expression in macrophage, we selected the Mac3-positive area and detected the signal intensity of p53, TRX, and DNMT3a in the Mac3-positive area. We used IgG control in place of each primary antibody with a section of each tissue sample to evaluate nonspecific staining. The area surrounded by the white dashed lines were designated as the Mac3-positive area. In Mac3-positive MC areas in the plaques (white dashed lines), p53 expression **(A)** was lower (n=6, 5) and TRX expression **(B)** (n=6, 5) and DNMT3a expression **(C)** (n=5, 7) were higher in ERK5 S496A KI cells than in WT cells. Scale bar=100 μm. Data are expressed as mean±SD. **(D)** Single-cell expression level of each marker in EC-like clusters between WT and ERK5 S496A KI plaques. TRX expression levels in #3 and #7; DNMT3a and GAS6 in #5, and #6; TYRO3 in #6; and IL-6 in #5 were increased in ERK5 S496A KI cells compared to in WT cells. We did not detect any differences in the expression of p53 and TOP2β between WT and ERK5 S496A KI. The Y-axis indicates the mean intensity, and black solid lines indicate the median value in each violin plot. Statistical significance was assessed by the Mann-Whitney test (n=2,536, 1,775 in cluster #5 and n=122, 202 in cluster #6). **(E)** The distance between the ECs in cluster #5 and the cells in each MC-like cluster was calculated by VIS software in the IMC analysis. The distance between EC-like cluster #5 and MC-like cluster #8 was shorter in ERK5 S496A KI cells than in WT cells (n=2484, 1781). Black solid lines indicate the median value in the violin plot. Statistical significance was assessed by the Mann-Whitney test. The images show EC-like cluster #5 and MC-like cluster #8 in WT (left) and ERK5 S496A KI (right) cells. White dashed lines indicate the surface of the plaque. L: lumen. Scale bar=100 μm**. (F)** BMDMs

migration was determined in the Boyden chamber system after seeding BMDMs in the upper insert and the addition of oxLDL (10 μg/ml) in the lower chamber. Analysis of BMDMs migration (number of migrating cells per field) for each group. **(G)** p16, p-TERF2IP, and p53 expression in MC (n=14,069 cells). The Y-axis indicates the mean intensity, and solid black lines indicate the median value in each violin plot. **(H)** Single-cell analysis of p16 and Ki67 expression in MC *in vivo* (left upper panel). The log scaled ratio of Ki67 and p16 of selected cells by $\log_{10}$(expression of Ki67/ expression of p16), and the cutoff of ratio with $\log_{10}$(-0.072) (left lower panel). The single-cell expression level of p-PKCζ and p16 between WT and ERK5 S496A KI plaque tissues (right panels). **(I, J)** Single-cell analysis of p53 and Ki67 expression in $CD31^+$ cells (I, n=4,635 cells) and α-SMA^+ cells (G, n=1,276 cells) *in vivo* (upper panels). The log scaled ratio of Ki67 and p53 of selected cells by $\log_{10}$(expression of Ki67/ expression of p53) (lower panels), and the cutoff of ratio with $\log_{10}$(-0.633) (J, left lower panel). Although the linear equation of p53 and ki67 in ECs is y=1.07x+0.26, R2 = 0.08 suggests that the correlation of p53 and Ki67 in ECs is very low. **(K)** The single-cell expression level of each marker in α-SMA^+ cells clusters between WT (n=687 cells) and ERK5 S496A KI (n=589 cells) plaque tissues. The Y-axis indicates the mean intensity, and solid black lines indicate the median value in each violin plot. The applied statistical tests, sample number, and results in all figures are summarized in Table S3.

Supplementary Figure 3. Role of ERK5 S496 phosphorylation in hypercholesterolemia-induced MCs reprogramming to SASP in *ex vivo* (Quantification of Figure 3F).

The graphs represent densitometry data from 5 independent gels, one of which is shown in Figure 3F. The applied statistical tests, sample number, and results in all figures are summarized in Table S3. The data are mean±SD, $^{**}P<0.01$, $^{*}P<0.05$.

Supplementary Figure 4. Macrophage polarization and cytokines secretion.

(A, B) Indicated mRNA levels were detected by qRT-PCR in BMDMs isolated from WT and ERK5 S496A KI mice fed with NCD or HFD *ex vivo*. **(C)** Cytokine profiling in mouse serum from WT and ERK5 S496A KI mice after 4 months of HFD and AAV-PCSK9 injection was detected by Mouse Inflammatory Array (AAM-INF-1-4, Ray Biotech, Inc) *in vivo*. The applied statistical tests, sample number, and results in all figures are summarized in Table S3. The data are mean±SD, $^{**}P<0.01$, $^{*}P<0.05$.

Supplementary Figure 5. Role of ERK5 S496 phosphorylation in hypercholesterolemia-induced mitochondrial dysfunction *ex vivo*.

BMDMs isolated from WT and ERK5S496A KI mice fed with NCD or HFD were seeded on Seahorse plates. After 24 hours, OXPHOS and glycolysis parameters were measured. During extracellular flux analysis, cells were sequentially treated with **(A)** oligomycin (OM), carbonyl cyanide 4-(trifluoromethoxy) phenylhydrazone (FCCP), and rotenone plus antimycin A (ROT/AA) and used to assess OXPHOS parameters based on oxygen consumption rates. **(B)** The basal respiration, mt ATP production, maximal respiration, and spare respiratory capacity were calculated and plotted as oxygen consumption rates in pmoles/minutes. **(C)** Glucose (GLUC), OM, and 2-deoxyglucose (2-DG) were used to determine glycolysis parameters from extracellular acidification rates. **(D)** Glycolysis, glycolytic reserve, glycolytic capacity, and non-glycolytic acidification were calculated and plotted as

the extracellular acidification rate in mpH/minutes. The applied statistical tests, sample number, and results in all figures are summarized in Table S3. The data in A and C are mean±SEM, and B and D are mean±SD, $**P<0.01$, $*P<0.05$.

Supplemental Figure 6. GO pathway analysis, enrichment plot, and GOBubble plot *ex vivo*.

(A) GO and pathway analysis of DEGs. Top 15 significant GO terms (biological processes) associated with the identified DEGs. The vertical axis represents the GO category, and the horizontal axis represents the *P*-value of the significant GO terms. **(B)** Enrichment plots from GESA. GESA results showing G2M checkpoint and UV Response DN (genes downregulated in response to ultraviolet (UV) radiation). **(C)** Bubble plot indicates significantly enriched GO terms for the differentially expressed DEGs only in WT HFD and ERK5 S496A KI HFD mice. Size of the bubbles is proportional to the number of DEGs (adj. p value <0.05) assigned to the GO term. The y-ais represents the negative logarithm of the adjusted p value (false discovery rate) for the GO terms, and the x-axis displays the z-score as calculated using the GOplot R-package[37]. The threshold for displaying the bubble labels was set to a log(FDR) of 1.0. Go terms belonging to biological process are green, molecular function are blue, and cellular component are red. **(D)** The graphs represent densitometry data from 3 independent gels, one of which is shown in Fig. 5I. The applied statistical tests, sample number, and results in all figures are summarized in Table S3. The data are mean±SD, n=5, $**P<0.01$.

Supplemental Figure 7. NRF2 K518 SUMOylation mediated by ERK5 S496 phosphorylation inhibits SASP induction *in vitro* (Quantification of Figure 5).

The graphs represent densitometry data from 5 independent gels, one of which is shown in Figure 5. The applied statistical tests, sample number, and results in all figures are summarized in Table S3. The data are mean±SD, $**P<0.01$, $*P<0.05$.

Supplemental Figure 8. NRF2 K518 SUMOylation mediated by ERK5 S496 phosphorylation inhibits SASP induction (Quantification of Figure 6J).

(A-B) BMDMs isolated from WT and ERK5S496A KI mice fed with NCD or HFD for 4 months were cultured with same medium. Cell lysates were immunoprecipitated with anti-NRF2 and immunoblotted with indicated antibodies *ex vivo*. Representative images from 3 independent experiments are shown. **(B)** The graphs represent densitometry data from 3 independent gels, one of which is shown in A. **(C)** The graphs represent densitometry data from 5 independent gels, one of which is shown in Figure 6J. The applied statistical tests, sample number, and results in all figures are summarized in Table S3. The data are mean±SD, $**P<0.01$.

Supplementary Table 1. Antibody panel for IMC

	Antigen	Vendor	Cat#	Metal tag
Endothelial cells	CD31	R&D	AF3628	143Nd
	p-Tyrosine	Fluidigm	3144024D	144Nd
Myeloid cells	CD107b	Invitrogen	14-1072-85	145Nd
	TOP2β	R&D	MAB6348	147Sm
Vascular smooth muscle cells	α-SMA	Fluidigm	3141017D	141Pr
Antioxidant	Thioredoxin (Trx)	Proteintech	14999-1-AP	148Nd
Myeloid cells	CD11b	Fluidigm	3149028D	149Sm
	p-PKCζ (T410)	Abclonal	AP0520	150Nd
	p-TERF2IP (S205)	Homemade		151Eu
Anti-inflammation	p-AMPK alpha (T172)	Affinity Biosciences	AF3423	152Sm
Chemotaxis	CCR7	Biorbyt	orb547290	155Gd
Efferocytosis	Tyro3	R&D	MAB759	156Gd
Efferocytosis	Gas6	Abclonal	A8545	158Gd
	p90RSK1	StressMarq	SPC-147F	159Tb
	p-p90RSK (S380)	Bioworld	BS4870	160Gd
Endothelial cells	ERG	Biorbyt	orb192164	161Dy
Senescence	p16	Abcam	ab54210	162Dy
Inflammation	IL-6	R&D	AF-406-NA	163Dy
M2 marker	Arginase-1	Fluidigm	3164027D	164Dy
Senescence	p53	Abcam	ab131442	165Ho
Endothelial cells	vWF	Millipore	AB7356	166Er
Proliferation	Ki67	Fluidigm	3168022D	168Er
CH driver	DNMT3a	Novus	NB120-13888	170Er
	p-ERK1/2	Fluidigm	3171021D	171Yb
CH driver	p-JAK2	Abcam	ab219728	173Yb
	YAP	Abcam	ab56701	174Yb
	p-YAP (Y357)	Abcam	ab62751	175Lu
DNA	Ir DNA-intercalator	Fluidigm	201192A	191Ir
DNA	Ir DNA-intercalator	Fluidigm	201192A	193Ir

RRID number for each antibody was described in Supplementary Table 5.

Supplementary Table 2. List of Real-time PCR primers.

Primers Sequences
IL-1β -F 5'-CTACAGGCTCCGAGATGAACAA-3'
IL-1β-R 5'-TCCATTGAGGTGGAGAGCTTTC-3'
TNFα-F 5'-GGCTGCCCCGACTACGT-3'
TNFα-R- 5'-AGGTTGACTTTCTCCTGGTATGA-3'
β-ACTIN-F 5'-AGAGGGAAATCGTGCGTGAC-3'
β-ACTIN-R 5'-CAATAGTGATGACCTGGCCGT-3'
iNOS-F 5'-TCCTGGAGGAAGTGGGCCGAAG3'
iNOS-R 5′-CCTCCACGGGCCCGGTACTC-3′
Arg1-F 5′-CAGAAGA- ATGGAAGAGTCAG-3′
Arg1-R 5′-CAGATATGCAGGGAGTCAC- C-3′
Ym1-F 5′-GCAGAAGCTCTCCAGAAGCAATCCTG-3

Ym1- R 5′-ATTGGCCTGTCCTTAGCCCAACTG-3′
Fizz1-F 5′-GCTGATGGTCCCAGTGAATAC-3
Fizz1-R 5′-CCAGTAGCAGTC- ATCCCAGC-3

Supplementary Table 3. The applied statistical methods and results for each figure.

Supplementary Table 4. Controls for each relative value.

Supplementary Table 5. RRID number for each antibody, cells, software tools, mice, and plasmids.

Major Resources Table

Raw data

File 1. The intensity of each protein in myeloid cells (MCs)-like cells in the plaques from hypercholesterolemia wild type and ERK5 S496A KI mice fed a high-fat diet.

Wild type mice (Mouse A-G, cell number #1-7903) and ERK5 S496A KI mice (Mouse H-M, cell number #7904-14069) raw intensity data were shown.

File 2. The intensity of each protein (Fig. S2D, I) in endothelial cells (ECs)-like cells in the plaques from hypercholesterolemia wild type and ERK5 S496A KI mice fed a high-fat diet.

File 3. The intensity of each protein (Fig. S2J, K) in α-SMA$^+$ cells in the plaques from hypercholesterolemia wild type and ERK5 S496A KI mice fed a high-fat diet.

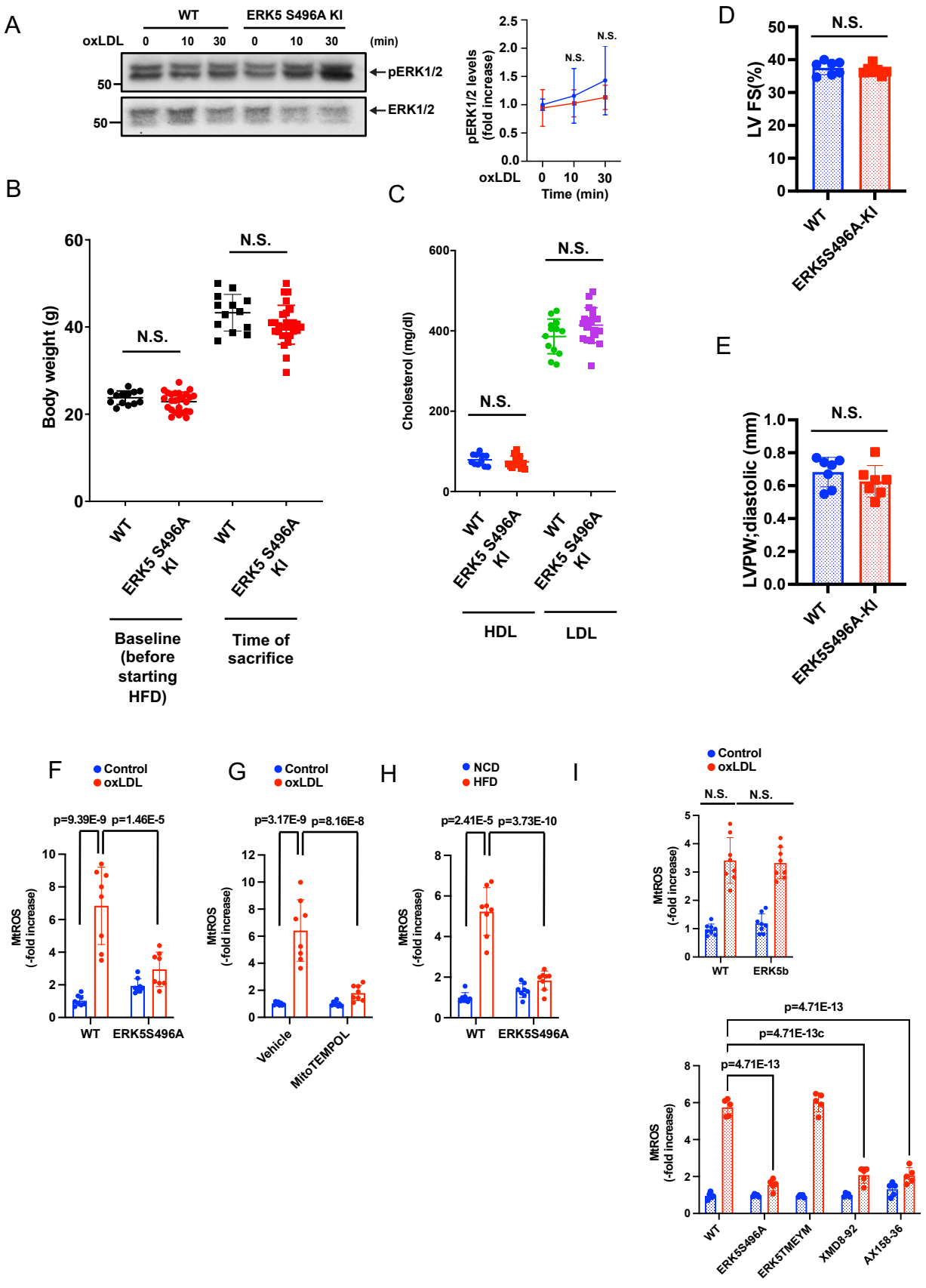

Supplementary Figure 1

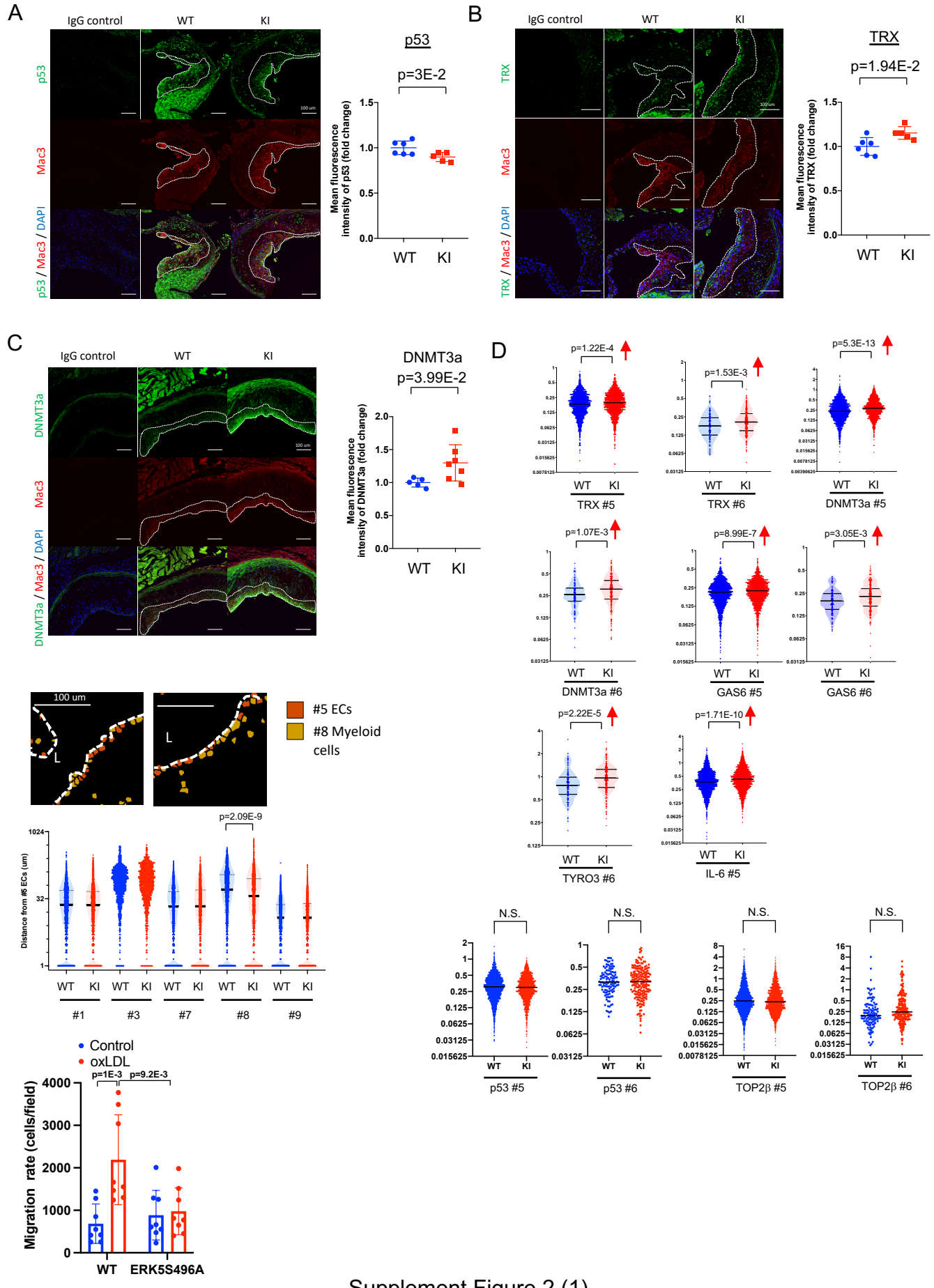

Supplement Figure 2 (1)

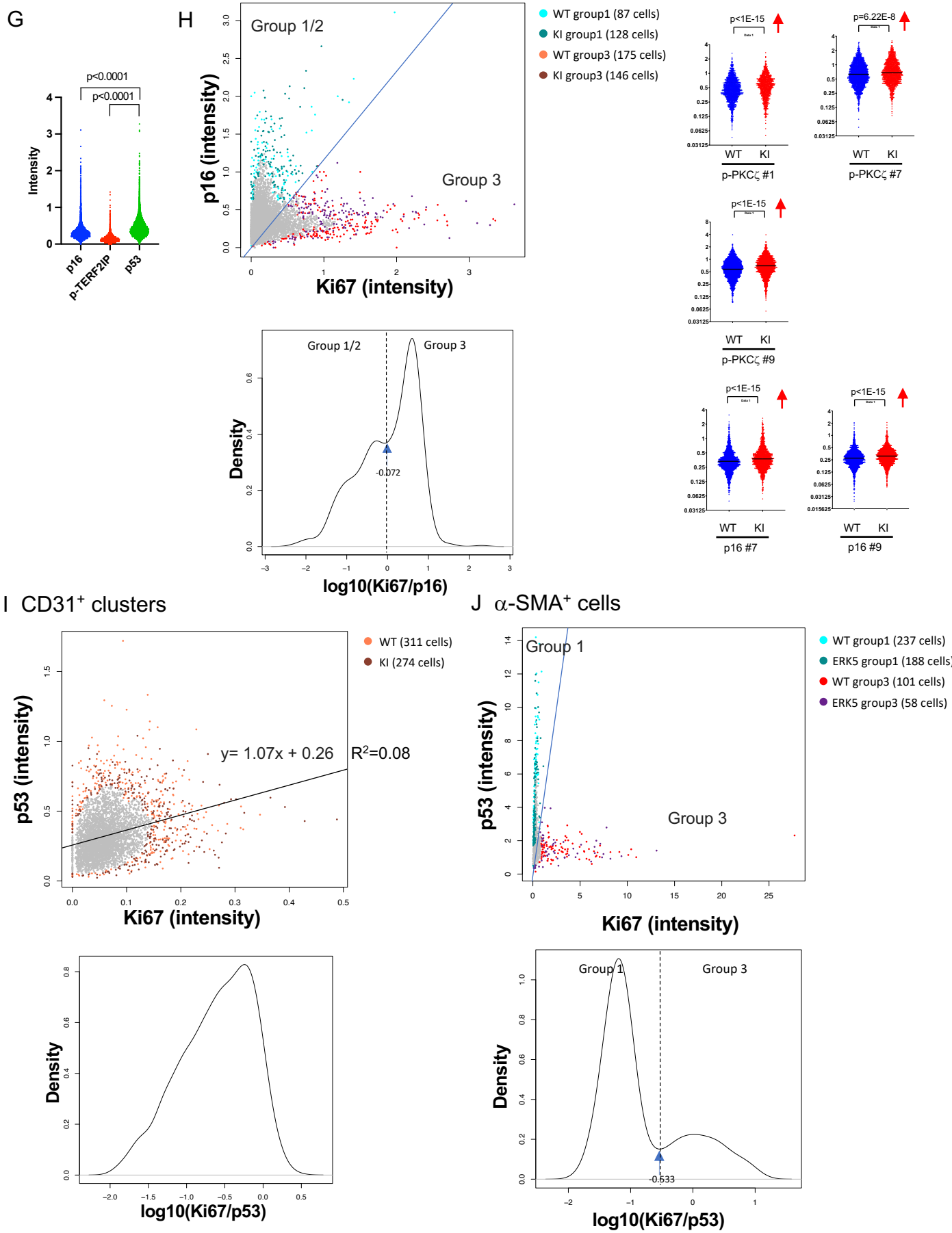

Supplement Figure 2 (2)

K

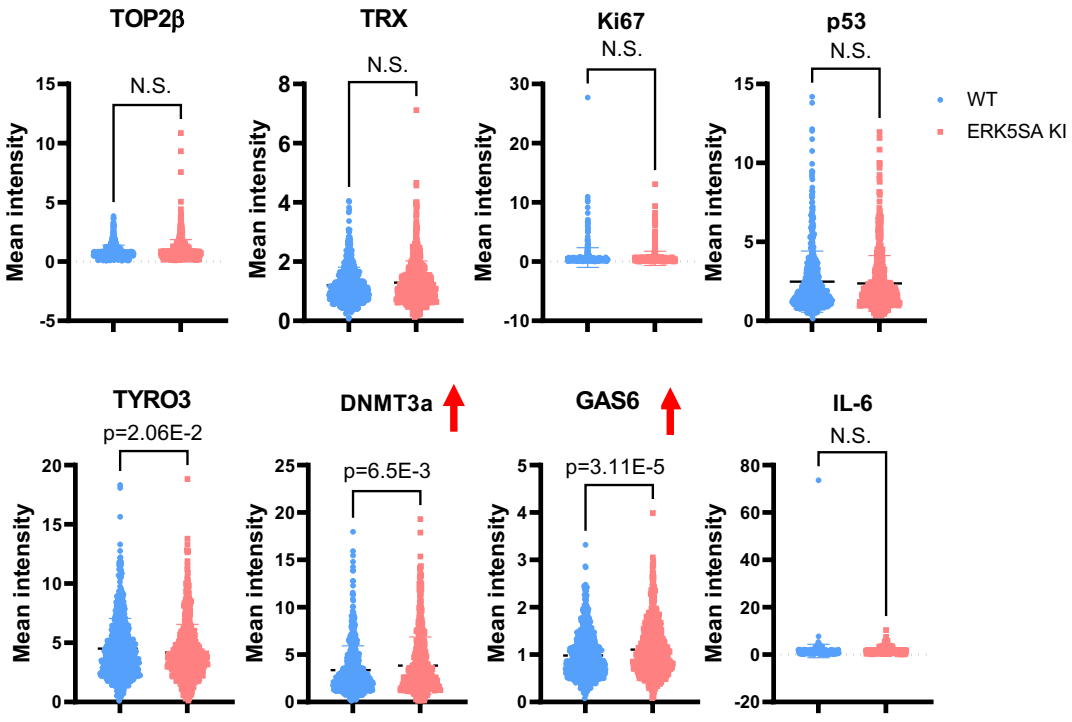

Supplement Figure 2 (3)

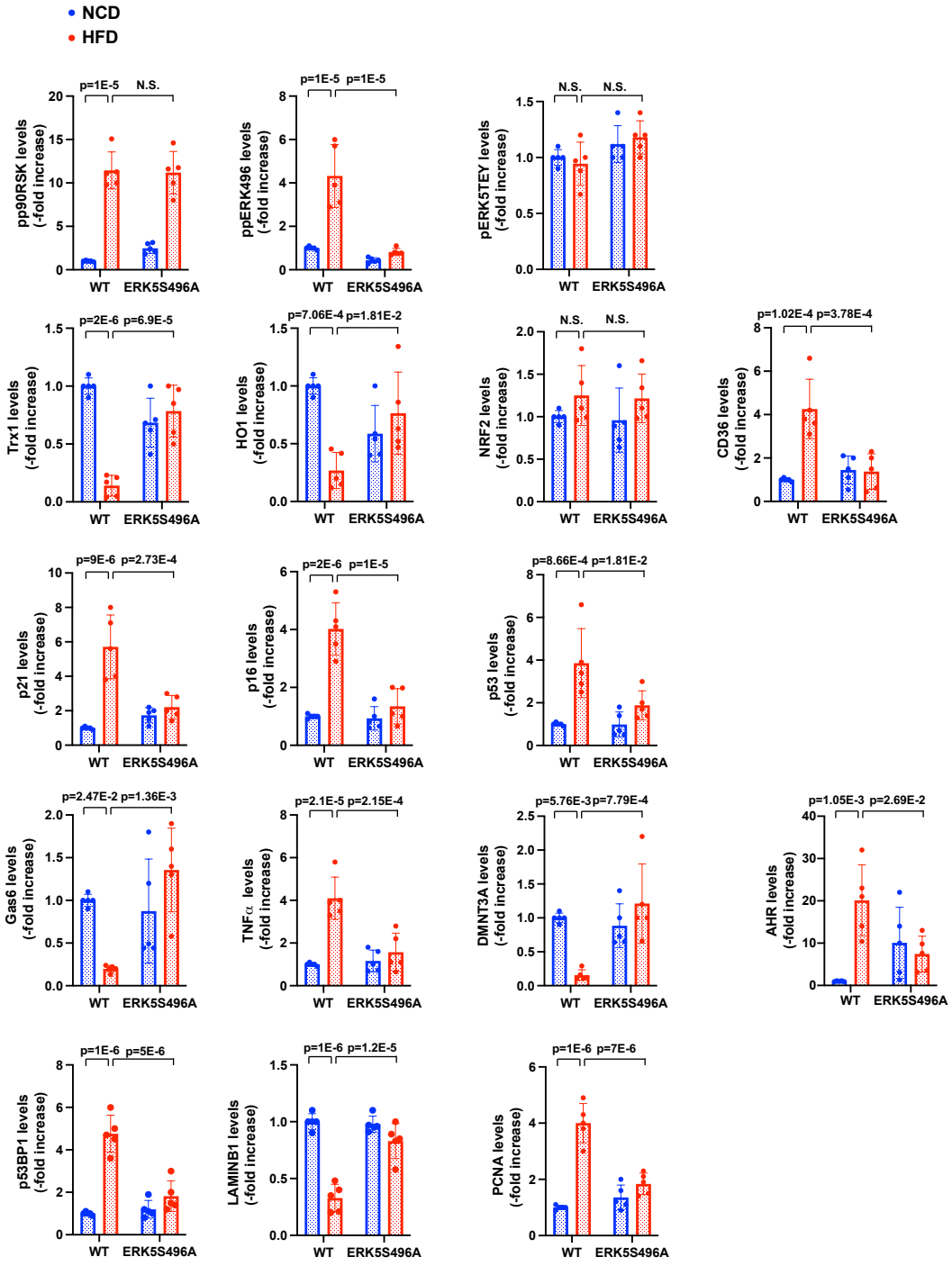

Supplement Figure 3

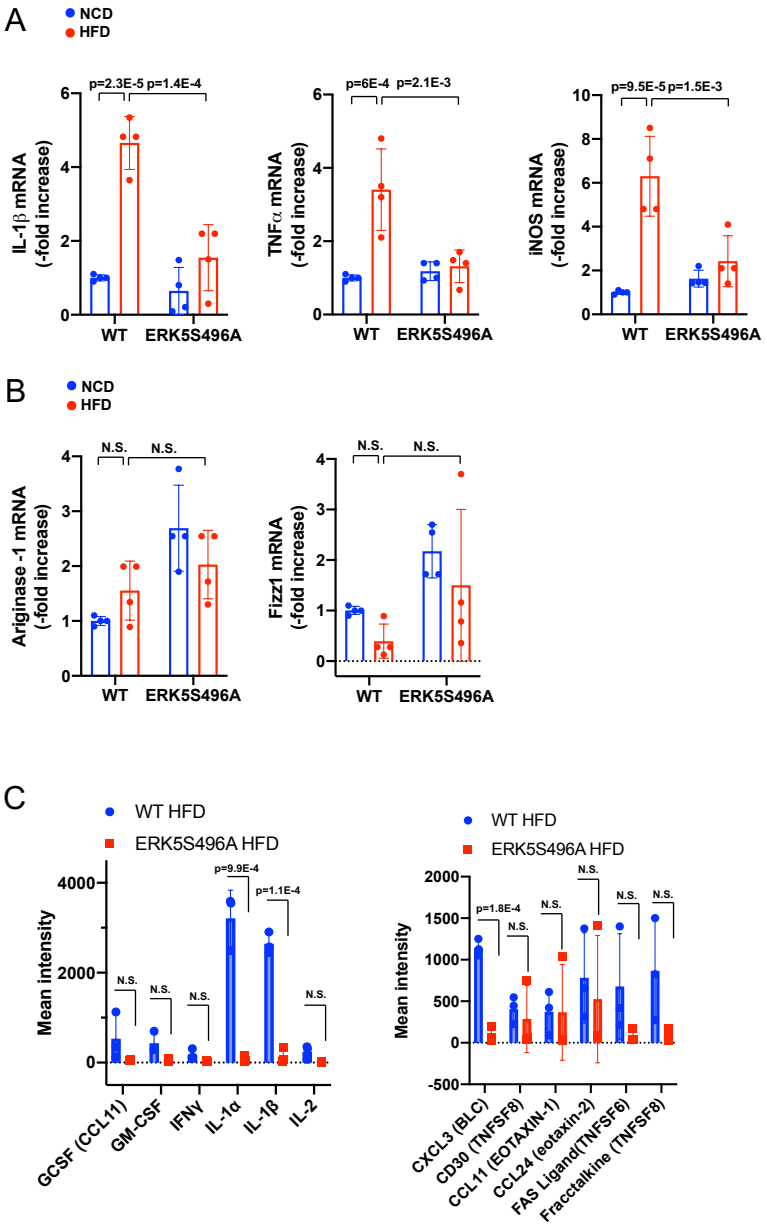

Supplement Figure 4

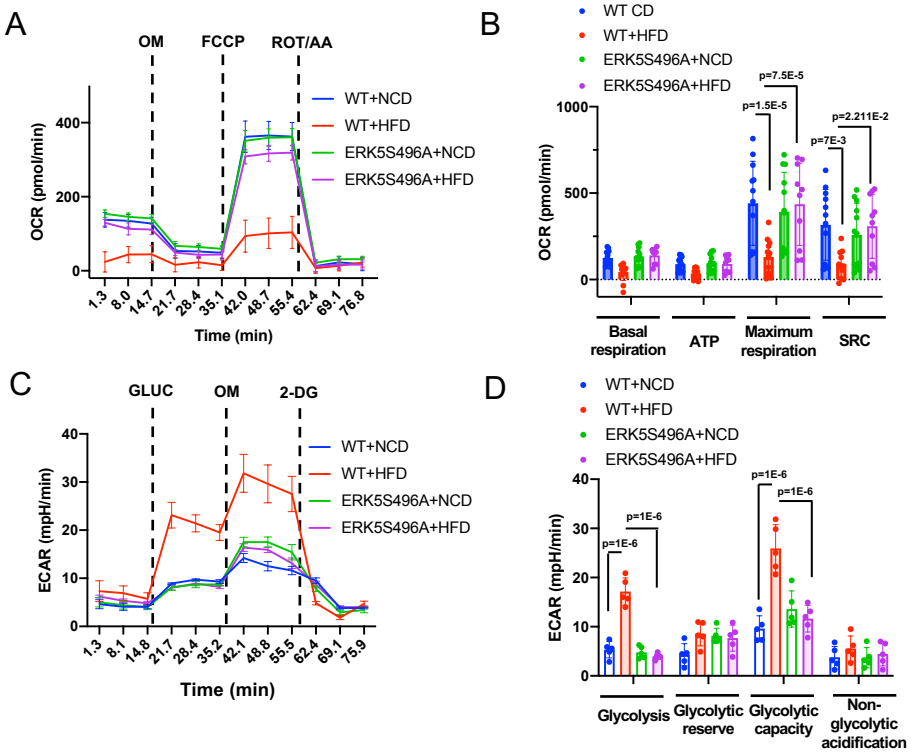

Supplement Figure 5

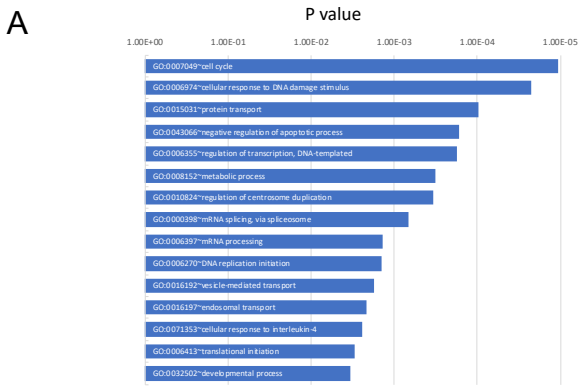

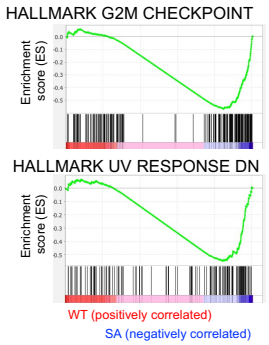

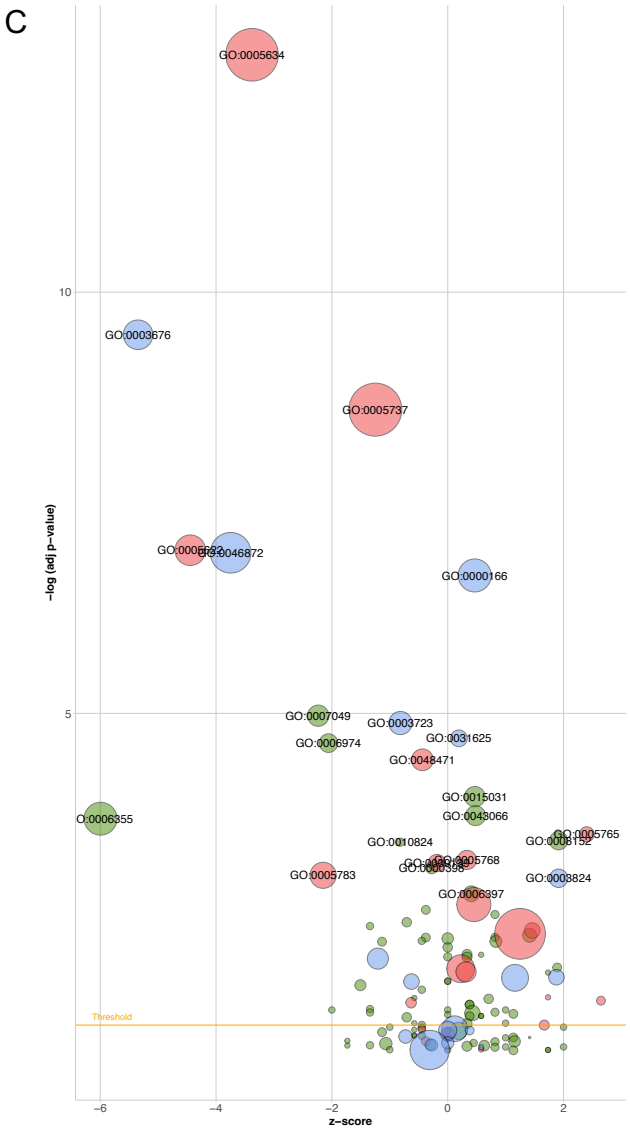

ID	Description
GO:0007049	cell cycle
GO:0006974	cellular response to DNA damage stimulus
GO:0015031	protein transport
GO:0043066	negative regulation of apoptotic process
GO:0006355	regulation of transcription, DNA–templated
GO:0008152	metabolic process
GO:0010824	regulation of centrosome duplication
GO:0000398	mRNA splicing, via spliceosome
GO:0006397	mRNA processing
GO:0005634	nucleus
GO:0005737	cytoplasm
GO:0005622	intracellular
GO:0048471	perinuclear region of cytoplasm
GO:0005765	lysosomal membrane
GO:0005768	endosome
GO:0000139	Golgi membrane
GO:0005783	endoplasmic reticulum
GO:0003676	nucleic acid binding
GO:0046872	metal ion binding
GO:0000166	nucleotide binding
GO:0003723	RNA binding
GO:0031625	ubiquitin protein ligase binding
GO:0003824	catalytic activity

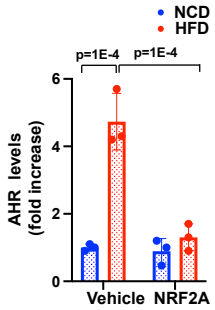

Supplement Figure 6

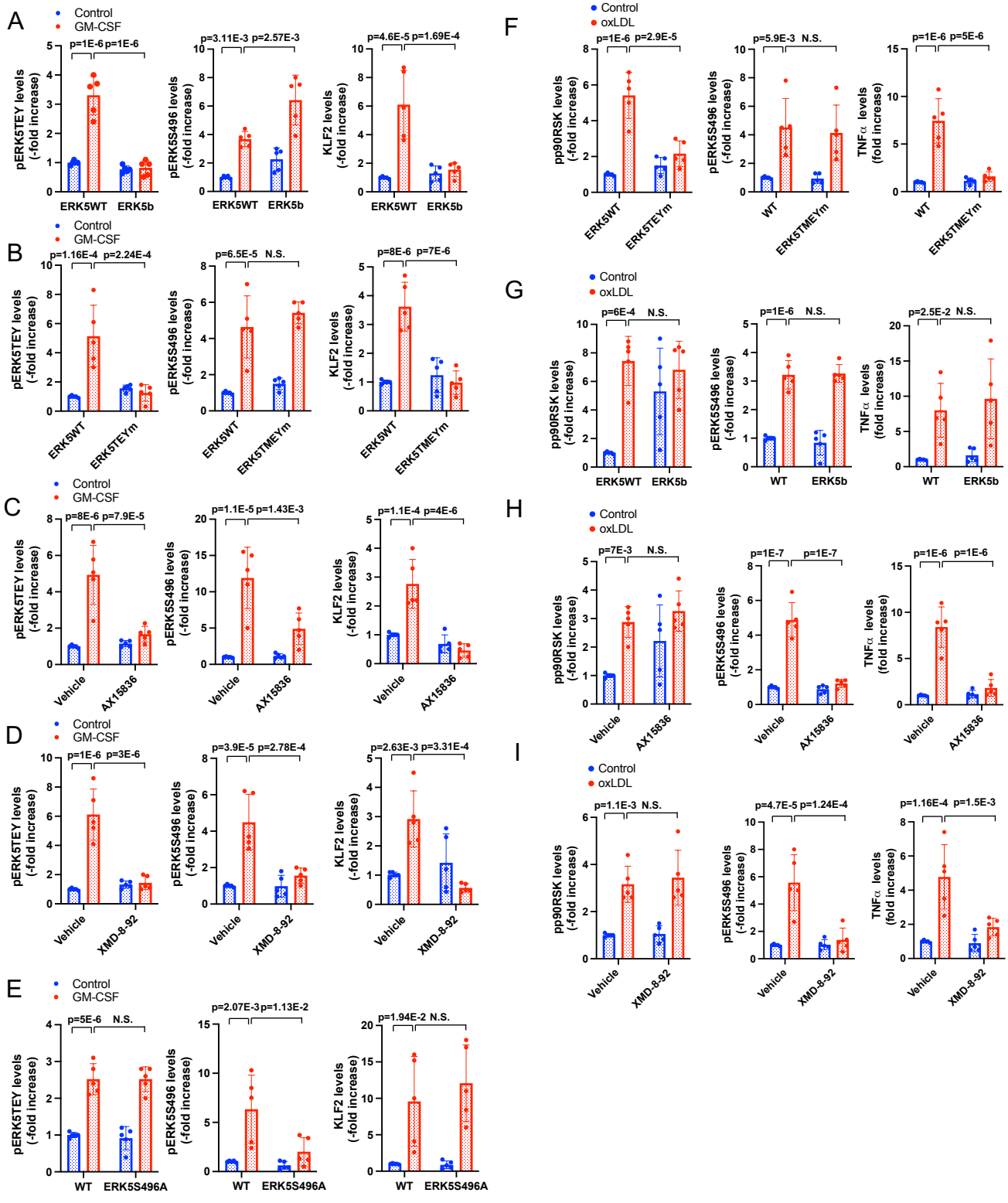

Supplement Figure 7

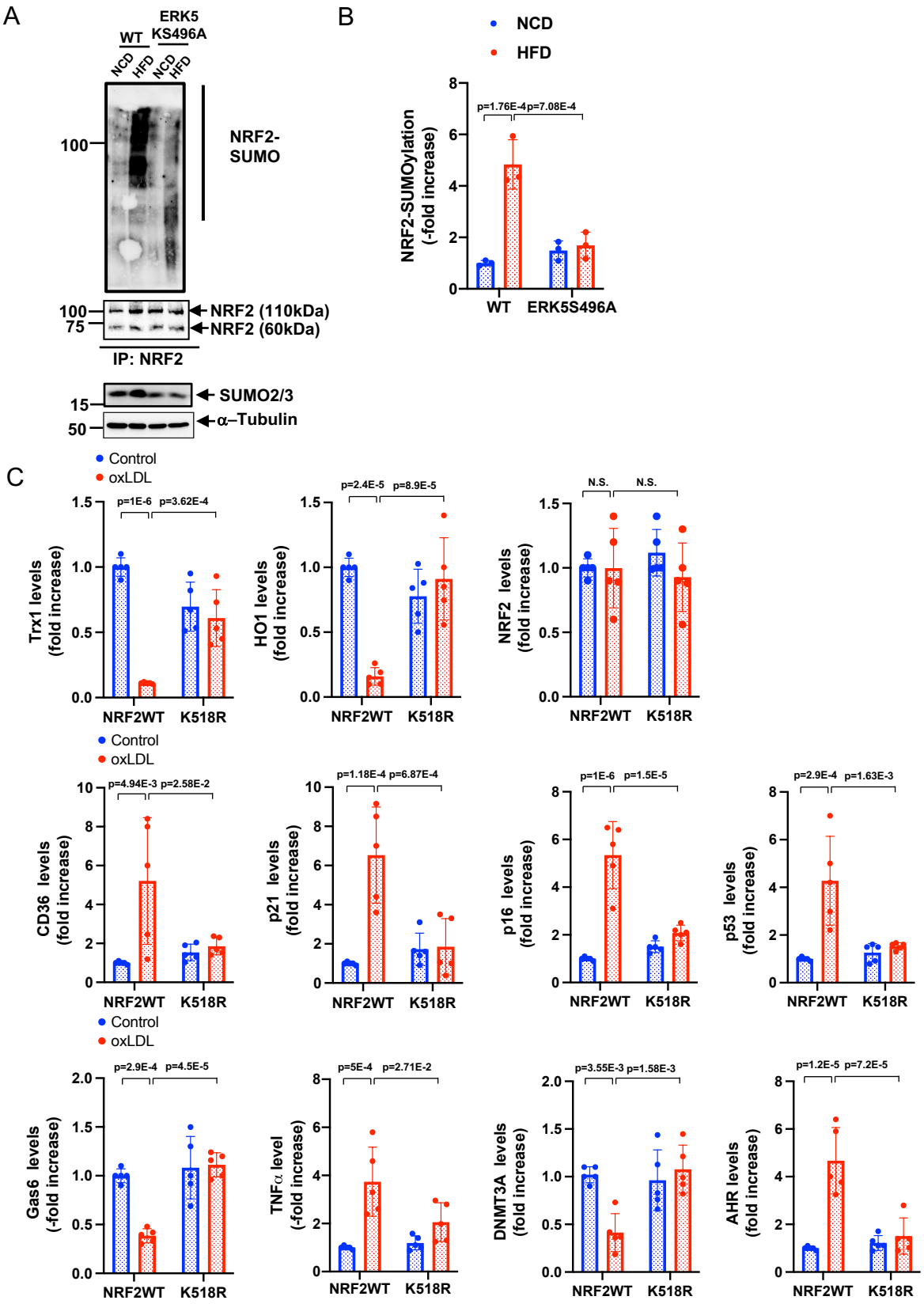

Supplement Figure 8